

Quantum entanglement, local indicators, and the effect of external fields in the Kugel-Khomskii model

V. E. Valiulin ^{*}, A. V. Mikheyenkov, and N. M. Chtchelkatchev

Moscow Institute of Physics and Technology, National Research University, Dolgoprudny 141701, Russia and Institute for High Pressure Physics, Russian Academy of Sciences, Moscow (Troitsk) 108840, Russia

K. I. Kugel

Institute for Theoretical and Applied Electrodynamics, Russian Academy of Sciences, Moscow 125412, Russia and National Research University, Higher School of Economics, Moscow 101000, Russia



(Received 24 July 2020; revised 27 September 2020; accepted 28 September 2020; published 19 October 2020)

Using the exact diagonalization technique, we determine the energy spectrum and wave functions for finite chains described by the two-spin (Kugel-Khomskii) model with different types of intersubsystem exchange terms. The obtained solutions provide the possibility to address the problem of quantum entanglement inherent in this class of models. We put the main emphasis on the calculations of the concurrence treated as an adequate numerical measure of the entanglement. We also analyze the behavior of two-site correlation functions considered a local indicator of entanglement. We construct the phase diagrams of the models involving the regions of nonzero entanglement. The pronounced effect of external fields, conjugated to both spin variables in the regions with entanglement, could both enhance and weaken the entanglement depending on the parameters of the models.

DOI: [10.1103/PhysRevB.102.155125](https://doi.org/10.1103/PhysRevB.102.155125)

I. INTRODUCTION

Entanglement is one of the main manifestations of the quantum nature of the matter being intensively studied in connection with the development of quantum computers [1–13]. The problem of entanglement has been studied in detail for nanosystems, especially for quantum dots [14]. Such systems are used for the design of quantum information processing systems.

In solids, which are traditional for condensed-matter physics, things are not so clear. Many standard solid-state systems are entangled. There can be no doubt that electrons in a metal are entangled [15], but how to verify this directly experimentally, using the accepted criteria, is the question. The conventional method for determining entanglement (we do not mention here Bell inequalities [16,17], which are very efficient in optics but not in solids, and other exotic methods) involves the determination of the density matrix, which is quite computationally problematic, even for a relatively small cluster. The most promising would be to extract information about entanglement from correlation functions related directly to the system at hand. There are many efficient methods for calculating correlation functions, both numerically and analytically, for strongly correlated systems with a large number of degrees of freedom, in particular, in the thermodynamic limit. Moreover, many correlators are experimentally determined. Another important issue is how one can manage the degree of entanglement. The influence of external fields on

entanglement is crucial here since it provides the possibility to control an entangled system in quantum information processing. We note that these fields may be of a completely different nature: from the magnetic field to elastic stresses.

The most vivid example of the entanglement in condensed matter is represented by the models involving two kinds of interacting spin variables. Two-spin models themselves usually appear in the description of specific features of transition metal compounds with coupled spin and orbital degrees of freedom; that is why such models are often referred to as spin-orbital ones (sometimes, the term Kugel-Khomskii model is used) [18–20]. Unusual effects related to the spin-orbital correlations and the corresponding quantum entanglement are widely discussed in the current literature. In particular, the possibility of extraordinary spin-orbital quantum states and transitions between them was pointed out [21–27].

The simplest version of the Kugel-Khomskii model, the $SU(2) \times SU(2)$ model with $SU(2)$ symmetries for both spin-1/2 and pseudospin-1/2 operators (\hat{S} and \hat{T}) and a positive factor at spin-pseudospin interaction, was used in an early attempt in the context of the entanglement [28].

Later on, entanglement was sought in various other related models: $SU(2) \times XY$ [29], $SU(2) \times XXZ$ [30], and $SU(2) \times SU(2)$ with additional spin-orbit anisotropy [25]. Briefly, the results of this analysis amount to the detection and characterization of the significant entanglement area, the degree of entanglement (mainly through the von Neumann entropy), and sometimes an indication of the possible complex entangled excitations [31]. All the mentioned works estimate the entanglement, the phase boundaries, etc., numerically for finite chains.

*valiulin@phystech.edu

In contrast to the cited works, here, we focus on how to manage the degree of entanglement. This can be done by mixing different intrasubsystem and intersubsystem interactions and by applying and switching external fields. Here, we consider these two issues.

We consider several versions of the spin-orbital model with both symmetric and nonsymmetric spin-pseudospin interactions. We also introduce different kinds of external fields and study their effect on the entanglement. In addition, we show the relationship between the degree of entanglement and pair correlators between the orbital and spin degrees of freedom.

In general, the Hamiltonian of the model reads

$$\hat{\mathbf{H}} = \hat{\mathbf{H}}_s + \hat{\mathbf{H}}_t + \hat{\mathbf{H}}_{ts}. \quad (1)$$

Here, $\hat{\mathbf{H}}_s$ and $\hat{\mathbf{H}}_t$ are Heisenberg-type interactions in the spin pseudospin-spin subsystems:

$$\hat{\mathbf{H}}_s = J \sum_{(i,j)} \hat{\mathbf{S}}_i \hat{\mathbf{S}}_j, \quad \hat{\mathbf{H}}_t = I \sum_{(i,j)} \hat{\mathbf{T}}_i \hat{\mathbf{T}}_j, \quad (2)$$

and $\hat{\mathbf{H}}_{ts}$ is the interaction between subsystems. Depending on the compound and its symmetry, $\hat{\mathbf{H}}_{ts}$ can be written as

$$\hat{\mathbf{H}}_{ts}^{(1)} = K \sum_{(i,j)} (\hat{\mathbf{S}}_i \hat{\mathbf{S}}_j) (\hat{\mathbf{T}}_i \hat{\mathbf{T}}_j), \quad (3)$$

$$\hat{\mathbf{H}}_{ts}^{(2)} = K \sum_{(i,j)} (\hat{\mathbf{S}}_i \hat{\mathbf{S}}_j) (T_i^z T_j^z), \quad (4)$$

$$\hat{\mathbf{H}}_{ts}^{(3)} = K \sum_{(i,j)} (S_i^z S_j^z) (T_i^z T_j^z), \quad (5)$$

$$\hat{\mathbf{H}}_{ts}^{(4)} = K \sum_{(i,j)\alpha} (S_i^\alpha S_j^\alpha T_i^\alpha T_j^\alpha). \quad (6)$$

In (2)–(6) \mathbf{i}, \mathbf{j} are vectors of the nearest neighbors, and $\hat{\mathbf{S}}_i$ and $\hat{\mathbf{T}}_i$ are spin and pseudospin operators, related to orbital degrees of freedom. Hereafter, we consider the most common case where $S = 1/2$, $T = 1/2$. α is a spin and pseudospin component index.

Note here that a broad class of Hamiltonians of this type can be simulated not only in the framework of solid-state strongly correlated systems but also by ultracold atoms in traps [22,23]. In this case, the Kugel-Khomskii model may be applicable to the bosonic atoms with an integer spin. Note also that in transition metal compounds (such as ruthenates or vanadates), we are sometimes dealing with integer values of effective spin and orbital quantum numbers.

The additional terms in the Hamiltonian related to the presence of external magnetic fields in both subsystems can be written as

$$\hat{\mathbf{H}}_f = -\mathcal{H}_s \sum_i \hat{\mathbf{S}}_i^z - \mathcal{H}_t \sum_i \hat{\mathbf{T}}_i^z, \quad (7)$$

where \mathcal{H}_s and \mathcal{H}_t are fields in spin and pseudospin systems, respectively. An efficient magnetic field in a pseudospin system occurs, for example, as a result of the action of elastic stresses during uniaxial compression of a crystal. We note that in this model, in contrast to multisublattice magnets, the fields \mathcal{H}_s and \mathcal{H}_t can be steered in opposite directions. Moreover, hereafter, we consider also staggered fields in both subsystems.

The entanglement of the two systems can be determined if the density matrix is known. There are several quantitative criteria divided into two main courses. One is based on the calculation of von Neumann entropy [20,25,28,30,31], while the second one requires a partial trace of the density matrix by the degrees of freedom of one of the subsystems. We note right away that, qualitatively, all criteria give the same result. Nonetheless, they may differ quantitatively. Here, we use the so-called concurrence. Naturally, since we use the exact diagonalization of the Hamiltonian [32–36] method, any other criterion can also be calculated.

As mentioned, we study entanglement between two subsystems—spin and orbital. Concurrence [4] is defined as

$$C = \sqrt{2\{1 - \text{tr}_1[\text{tr}_2(\hat{\rho})^2]\}}, \quad (8)$$

where $\hat{\rho}$ is the density matrix of the entire system, $\text{tr}_i(\hat{\rho})$ is the partial trace of the density matrix in one of the subsystems, and i is the subsystem index (in our case, spin or pseudospin). Thus defined, concurrence for two single particles takes values from $C = 0$ in the absence of entanglement to $C = \sqrt{3}/2$ in the textbook Einstein-Podolsky-Rosen pair.

We compare the entanglement obtained in terms of the strict criterion based on C with the behavior of the local correlation functions of the operators $\hat{\mathbf{S}}_i$ and $\hat{\mathbf{T}}_j$. It turns out that paired correlators provide minimal information about entanglement, even if the operators belong to different sites. Moreover, the range of parameters where the state of the system is most entangled could be found with the correlators of the four operators, more precisely, their gradients.

Naturally, the inclusion of sufficiently high uniform external magnetic fields (7) suppresses entanglement. Nonetheless, in the range of interest, when the magnetic field has the same order of amplitude as the exchange integrals J, I, K , entanglement is not suppressed. Furthermore, as will be seen below, in some cases the external field surprisingly increases the entanglement. There is a dramatic change, however, in the regions with the strongest entanglement in the phase diagram. The most vivid effect is the shrinking of entanglement areas along specific directions or at points in the phase diagram under the influence of external fields.

II. METHODS

We consider the Kugel-Khomskii model (1) and (2) with the conventional symmetric spin-pseudospin interaction (3) and the related models with asymmetric [Eqs. (4) and (5)] and symmetric [Eq. (6)] interactions for a small linear cluster. We accurately determine the many-particle ground state wave function in the framework of the exact diagonalization method. The maximum cluster size is limited by computing resources; nevertheless, the key characteristics of the system are stable for variations in the chain size. We study the cases of both zero field and strong external field in each subsystem and focus mainly on how to manage the degree of entanglement.

This leads to a nontrivial and unobvious behavior of entanglement between spin and orbital degrees of freedom.

We have studied in detail one-dimensional systems with different boundary conditions: an open chain and a ring. For the whole range of the considered parameters, the open chain

appeared to be more convenient for calculation. In addition, as mentioned earlier, we consider mainly the case of nonzero external fields when the problem with the ground state accidental degeneracy is insignificant (for the zero-field limit we simply set relatively small fields). We should also note that the anisotropy [25] removes the problem even without external fields.

Hereinafter, we consider the open chain with the exact diagonalization method. We calculate the ground state wave function, which allows us to evaluate the von Neumann entropy, any entanglement criterion, and correlation functions in each subsystem and between them. The Hamiltonian matrices for the systems under study are very sparse, so it is natural to use the sparse matrix format. The maximum available size of the chain for comprehensive calculation is determined by the computational resources, mainly by the RAM size, so we extrapolate the results to $1/N \rightarrow 0$.

In our work, we have mainly used the QuTiP package, which simplifies the work with quantum objects [37,38]. In particular, the package has a convenient interface for constructing the many-particle Hamiltonian using a large number of direct products of various spin operators. All objects in the package are, by default, converted to sparse format, which significantly simplifies their further processing. The exact diagonalization procedure was performed in the QuTiP package as well. A typical calculation for a chain of ten sites for 3600 points takes about a day. Results for $N = 8, 9, 10$ slightly differ qualitatively and allow fine extrapolation to $1/N \rightarrow 0$. When possible, we compare the results with the earlier works on entanglement.

III. KUGEL-KHOMSKII MODEL WITH $\hat{H}_s = \sum (\hat{S}_i \hat{S}_j)(\hat{T}_i \hat{T}_j)$ INTERACTION

First, we consider the Kugel-Khomskii model (1) and (2) with the most common form (3) of spin-pseudospin interaction. We recall that in the mean field, all four common phases are realized: FM-FM, AFM-AFM, FM-AFM, and AFM-FM [39]. For large absolute values of $K < 0$ compared to I and J , this system prefers ferromagnetic (FM) or antiferromagnetic (AFM) ordering in both subsystems simultaneously. The opposite case, large $K > 0$, favors FM in one subsystem and AFM in the other.

For infinite system, quantum fluctuations destroy long-range order even at $T \rightarrow 0$, and the state structure is governed by the local order, i.e., correlation functions on distinct sites. We address a finite chain but, to avoid going into the redundant details, will mark different phases (technically, different local orders) by local correlation functions.

In the mean field, FM order in, e.g., the spin subsystem can be characterized by the unidirectional average of spins $\langle \hat{S}_i \rangle$, and AFM order can be characterized by a checkerboard pattern (in one-dimensional average spin directions altering from site to site). In terms of local correlators (irrespective of the long-range order) FM structure corresponds to $\langle \hat{S}_i \hat{S}_j \rangle > 0$ for any pair of sites. As for AFM, the sign of the correlation function $\langle \hat{S}_i \hat{S}_j \rangle$ is negative for nearest-neighbor sites \mathbf{i}, \mathbf{j} and changes when \mathbf{i} and \mathbf{j} take a step from one another. The same naturally holds for the pseudospin subsystem.

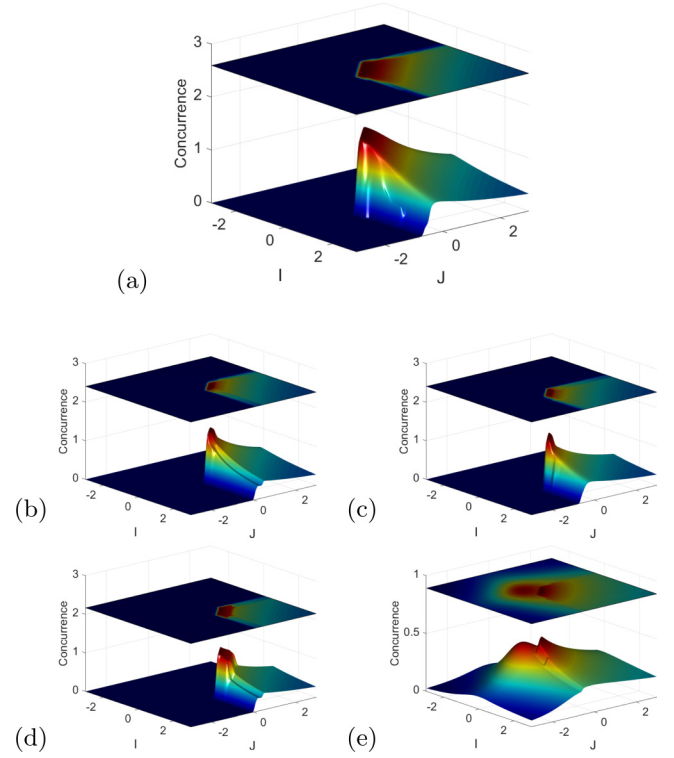


FIG. 1. Entanglement C (8) for intersubsystem exchange (3) $\sim (\hat{S}_i \hat{S}_j)(\hat{T}_i \hat{T}_j)$ with negative $K = -1$ and external fields. In contrast to the case of $K = +1$, here, the C maximum occurs not at a single point but at a segment of the diagonal line. (a) $\mathcal{H}_s = \mathcal{H}_t \ll 1$. (b) $\mathcal{H}_s = 1, \mathcal{H}_t \ll 1$. (c) $\mathcal{H}_s \ll 1, \mathcal{H}_t = 1$. (d) $\mathcal{H}_s = 1$ and $\mathcal{H}_t = 1$. (e) Staggered fields $|\mathcal{H}_s| = |\mathcal{H}_t| = 1$ in both subsystems. Here, \mathcal{H}_s and \mathcal{H}_t stand for external fields in spin and pseudospin subsystems.

In the quantum case, we adopt the following classification: FM, $\langle \hat{S}_i \hat{S}_j \rangle > 0$ for close neighbor pairs \mathbf{i}, \mathbf{j} , and AFM, $\langle \hat{S}_i \hat{S}_j \rangle < 0$ for nearest neighbors and altering thereafter. We do not deal with the exhaustive classification and the fine details of the state structure but, rather, superficially mark the local correlation. The foregoing does not necessarily mean the phase transitions with distinct order parameters but, rather, short-range order rearrangement.

Hereafter, we study how entanglement changes across local order boundaries, i.e., among the areas with different patterns of local correlations.

A. Entanglement and the sign of intersubsystem exchange K

We begin with the case of a negative intersubsystem exchange $K < 0$.

Figure 1(a) presents a measure of entanglement: concurrence C [see Eq. (8)] for negative intersubsystem exchange $K = -1$. As can be expected, nonzero entanglement is observed in the area of negative exchanges in both subsystems, and its maximum is achieved for comparable values of J, I , and K . This acknowledges that not only the binding interaction K between subsystems but also local interactions J and I are decisive for the entanglement. For $K > 0$ the same conclusion holds (see below).

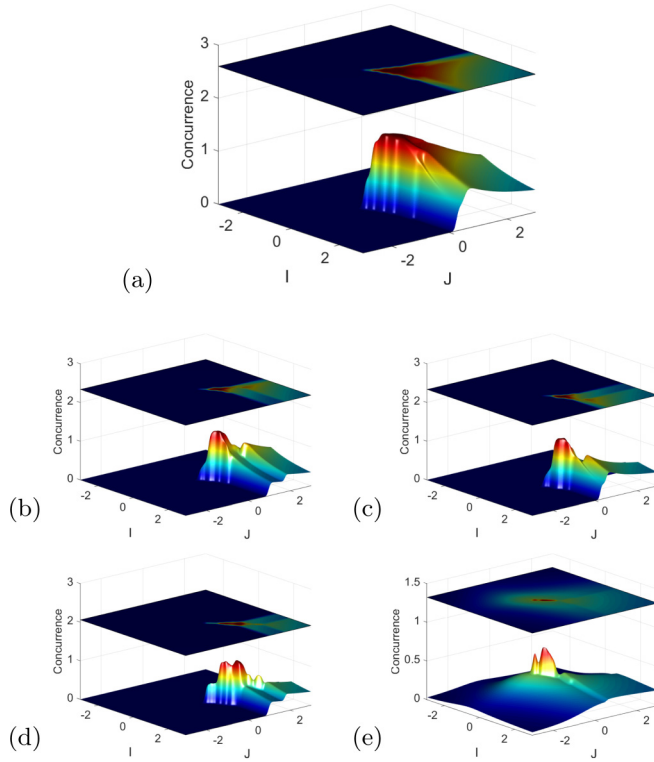


FIG. 2. Entanglement C (8) for intersubsystem exchange (3) $\sim (\hat{S}_i \hat{S}_j)(\hat{T}_i \hat{T}_j)$ with positive $K = +1$. The maximum entanglement is achieved at single point. (a) $\mathcal{H}_s = \mathcal{H}_l \ll 1$. (b) $\mathcal{H}_s = 1, \mathcal{H}_l \ll 1$. (c) $\mathcal{H}_s \ll 1, \mathcal{H}_l = 1$. (d) $\mathcal{H}_s = 1$ and $\mathcal{H}_l = 1$. (e) Staggered fields $|\mathcal{H}_s| = |\mathcal{H}_l| = 1$ in both subsystems. Here, \mathcal{H}_s and \mathcal{H}_l stand for external fields in spin and pseudospin subsystems.

For $K = -1$, the phase (local order) boundary and the structure of the C maximum differ significantly from the case with $K = +1$ [see Fig. 2(a)]. The maximum of entanglement arises at a segment, while for $K = +1$ it arises at a single point.

Figures 1(a) and 2(a) qualitatively reproduce the known results [28,31]. The spin-pseudospin structure in the finite-entanglement area corresponds to AFM spin and AFM pseudospin local orders (this is supported by the intersubsystem local correlation functions; see Sec. S1 of the Supplemental Material [40]). In Sec. IV, we discuss the interconnection of the entanglement and local correlators, which is much less studied, in depth.

It appears that nonzero external fields change the degree of entanglement in different ways. We will discuss this in more detail in Sec. III B. Nevertheless, let us first note once more that for both signs $K \geq 0$ the significant entanglement appears in the intuitive case of AFM exchanges in both subsystems, $J, I > 0$.

B. Entanglement and external fields

We now discuss the effect of external fields on the entanglement. Let us note once again that in the spin-orbital model different fields can be introduced in different subsystems, even if they act in opposite directions.

It is intuitive that sufficiently large external field suppresses the entanglement, as it strengthens the tendency to form a common ferromagnetic state. We will discuss below that the entanglement area transformation under strong external field is not so trivial, especially in the very frustrated case $J \sim I \sim K$, where entanglement typically has a maximum.

With a negative sign in the intersubsystem exchange, $K = -1$, the initial zero-field picture under the influence of an external field shifts, almost without deformation, along the corresponding coordinate axis [see Figs. 1(b) and 1(c)].

The case of two simultaneously acting fields is more peculiar. A local area of strong entanglement is formed, having a tooth shape [see Fig. 1(d)]. The result is practically independent of the mutual orientation of the fields. With magnification of the field amplitude, the localization effect increases, although is not transformed qualitatively, so we put the corresponding figure in Sec. S2 of the Supplemental Material [40].

The effect of the staggered fields (similar in both subsystems) is even more amazing [see Fig. 1(e)]. The area of substantial entanglement in the $J - I$ plane is dramatically enlarged, and the nonzero entanglement appears in the domains where it was negligible in all other cases under discussion.

Similar effects are observed with a positive sign in the intersubsystem exchange, $K = +1$. Here, also, the initial zero-field pattern under an external field shifts along the corresponding coordinate axis [see Figs. 2(b) and 2(c)]. Nevertheless, some deformation of the initial structure is observed with the nonmonotonic behavior of entanglement with increasing J or I .

With two simultaneously nonzero fields, as well as for $K = -1$, the local area of entanglement is formed [see Fig. 2(d)]. Moreover, the situation is almost unrelated to the mutual orientation of the fields, and as the field amplitude increases, the localization effect of a region of strong entanglement becomes more pronounced.

The destructive effect of the staggered fields in the case of positive $K = +1$ is much stronger than for $K = -1$ [see Fig. 2(e)]. Only a sharp narrow segment near $|J| \sim |I| \lesssim 1$ survives against the smooth concurrence background.

IV. INTERRELATION BETWEEN SPIN-PSEUDOSPIN CORRELATION FUNCTIONS AND ENTANGLEMENT

Correlation functions between spin (pseudospin) degrees of freedom provide important information about the system state structure. On the one hand, we can find the local structure in the spin and pseudospin subspace that allows us to roughly distinguish FM- and AFM-like local ordering. On the other hand, irreducible intersubsystem correlators may be sensitive to entanglement effects. We study this question in detail below.

It would be natural to expect a one-site intersubsystem correlator $\langle \hat{S}_i \hat{T}_i \rangle$ to be related to entanglement. Nevertheless, our analysis shows that in the general case, a chain-averaged single-site spin-pseudospin correlator does not provide accurate information about the entanglement region. For an example, compare Fig. 3(a) with Fig. 1(a): the single-site spin-pseudospin correlator reproduces only one small segment of

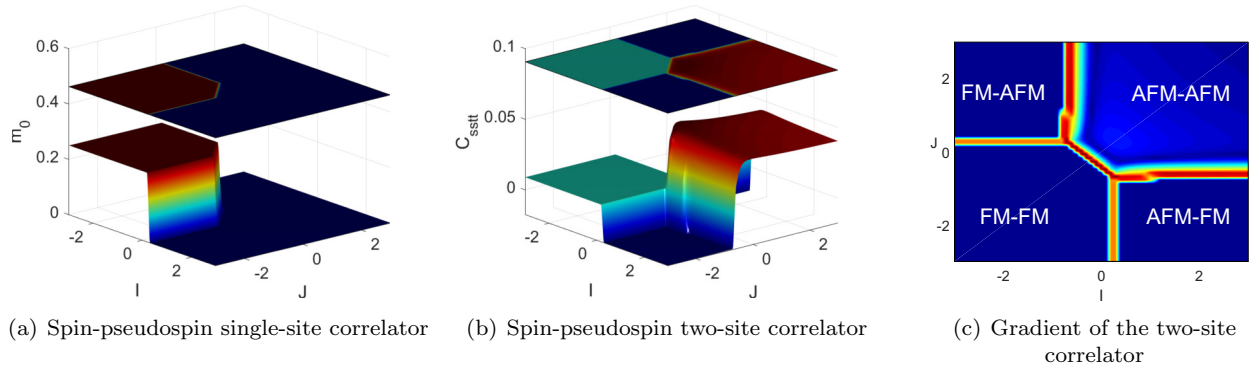


FIG. 3. $K = -1$. (a) The chain-averaged single-site spin-pseudospin correlator does not provide accurate information on the entanglement. (b) The two-site spin-pseudospin correlator reveals the entanglement region boundaries. (c) The gradient of the two-site correlator allows us to select the area of entanglement. The order structure in spin and pseudospin subsystems is designated.

the entanglement area borders (this is also the case for other types of intersystem interaction considered below).

Thus, one should address a two-site correlator: $\langle \hat{S}_i \hat{S}_j \hat{T}_i \hat{T}_j \rangle$. In Fig. 3(b), the two-site spin-pseudospin correlator $\langle \hat{S}_i \hat{S}_j \hat{T}_i \hat{T}_j \rangle$ (i, j are the nearest neighbors) is shown for $K = -1$. According to Fig. 1(a), the two-site spin-pseudospin correlator reasonably reproduces the entanglement region boundaries. Note that one-site and two-site irreducible correlators (covariances) $\langle \hat{S}_i \hat{T}_i \rangle - \langle \hat{S}_i \rangle \langle \hat{T}_i \rangle$, $\langle \hat{S}_i \hat{S}_j \hat{T}_i \hat{T}_j \rangle - \langle \hat{S}_i \hat{S}_j \rangle \langle \hat{T}_i \hat{T}_j \rangle$ lead to the same result for phase boundaries as the initial correlators.

A much clearer picture of the boundaries is visible in Fig. 3(c), where the gradient (in the parameter space) of a two-site spin-pseudospin correlator is presented. The gradient structure allows one to distinguish the entanglement in the phase diagram precisely.

In Fig. 4, similar data are shown for positive spin-pseudospin exchange $K = +1$. In Fig. 4(a), the single-site spin-pseudospin correlator does not provide information on the entanglement area [compare with Fig. 2(a)]. In Fig. 4(b), similar to Fig. 3(b), the two-site spin-pseudospin correlator reasonably reproduces boundaries of the entanglement region. Finally, the gradient of a two-site spin-pseudospin correlator selects the entanglement [Fig. 4(c)] accurately.

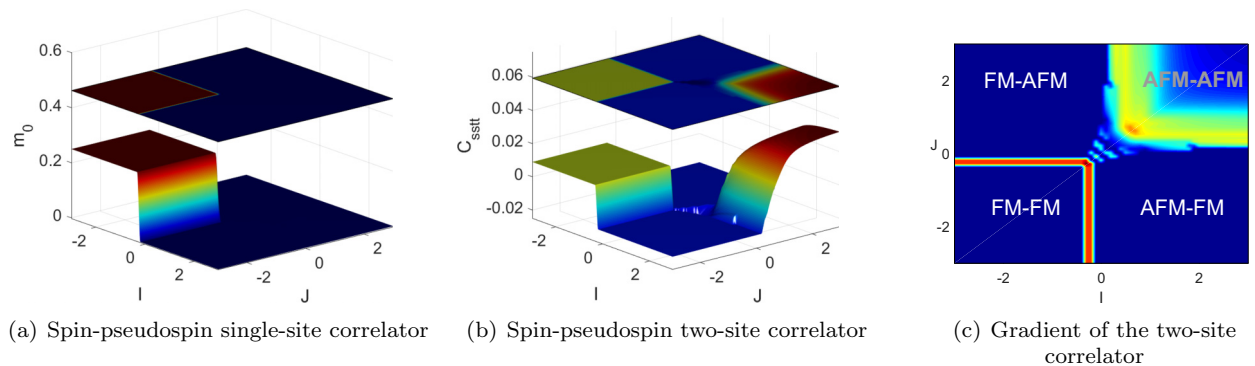


FIG. 4. $K = +1$. Analogous to Fig. 3. (a) The chain-averaged single-site spin-pseudospin correlator does not provide accurate information on the entanglement. (b) The two-site spin-pseudospin correlator reveals the entanglement region boundaries. (c) The gradient of the two-site correlator allows us to select the area of entanglement. The order structure in spin and pseudospin subsystems is designated.

Thus, in this section, we propose a criterion (purely empirical) for indicating the region of quantum entanglement in complex many-particle systems. It requires neither checking Bell's inequalities nor calculating the full density matrix. The corresponding two-site correlator can be determined either numerically, but with much less wasting of resources, or even analytically [24].

V. OTHER TYPES OF SPIN-PSEUDOSPIN INTERACTIONS

Hereinafter, we consider other possible types of spin-pseudospin interaction that up to now have not been investigated, at least in the context of entanglement.

A. Pseudospin anisotropic interaction: $\hat{H}_{ts} = \sum (\hat{S}_i \hat{S}_j)(T_i^z T_j^z)$

In this section, we consider what changes in the entanglement pattern entail a nontrivial, less symmetric spin-pseudospin interaction. This refers to the Hamiltonian (1) and (2) with the interaction between the subsystems (4)—Heisenberg-type interaction in \hat{H}_{ts} for spins and Ising-type interaction for pseudospins (note that this kind of interaction along with (3) was already proposed in the pioneering work on spin-orbital physics in compounds of transition metal elements [18]).

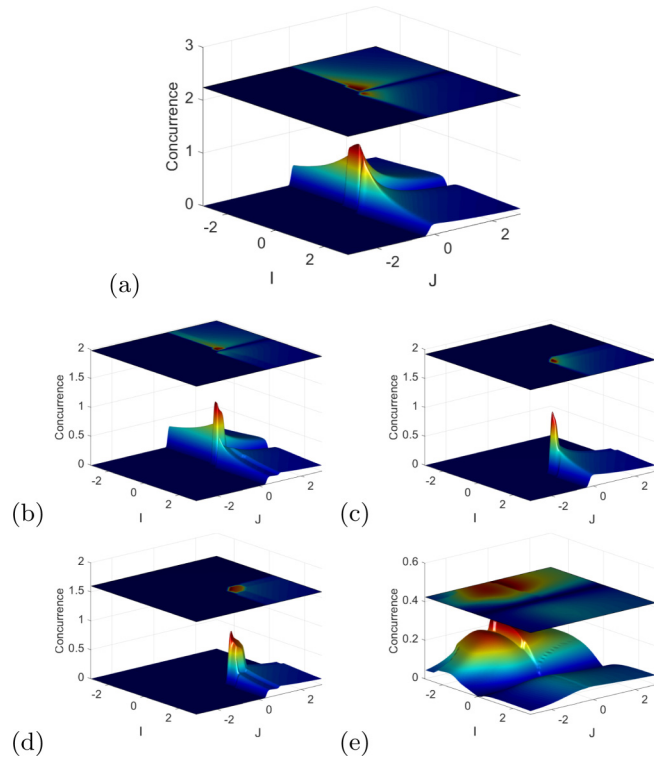


FIG. 5. Entanglement C (8) for intersubsystem exchange (4) $\sim (\hat{S}_i \hat{S}_j)(T_i^z T_j^z)$ with negative $K = -1$. At zero external fields, the entangled state is realized at half of the phase plane. (a) $\mathcal{H}_s = \mathcal{H}_t \ll 1$. (b) $\mathcal{H}_s = 1, \mathcal{H}_t \ll 1$. (c) $\mathcal{H}_s \ll 1, \mathcal{H}_t = 1$. (d) $\mathcal{H}_s = 1$ and $\mathcal{H}_t = 1$. (e) Staggered fields $|\mathcal{H}_s| = |\mathcal{H}_t| = 1$ in both subsystems. Here, \mathcal{H}_s and \mathcal{H}_t stand for external fields in spin and pseudospin subsystems.

The most dramatic changes occur in the case of the negative intersubsystem exchange constant $K = -1$. Here, in addition to the region $J, I \gtrsim 0$, a whole new region of significant entanglement C (8) arises [see Fig. 5(a)]. More than half of the investigated region is occupied by an entangled state separated by the trivial line $I = 0$.

For the other sign of the intersubsystem exchange constant, $K = +1$, there are no qualitative changes in the entanglement structure in Fig. 6(a) in comparison with the similar one in Fig. 2(a) for symmetric intersubsystem interaction (3). Here, the entanglement area is qualitatively the same; a distinct “shark tooth” is formed near the origin. On the other hand, quantitative changes in the fine structure are rather significant.

The response of the spin-orbital system to a nonzero field for $K = -1$ differs qualitatively from the previous case [see Figs. 1(b)–1(e)]. The picture does not change qualitatively when the external field is nonzero in the spin subsystem. Only a shift is observed along the corresponding coordinate axis [J ; Fig. 1(b)]. On the contrary, the external field in the pseudospin subsystem destroys the entangled state in a quarter of the phase plane [$J > 0, I < 0$; Fig. 1(c)]. If there is a nonzero external field in both subsystems, a sharp peak of entanglement is formed near the origin [see Fig. 1(d)]. As in Sec. III B, the mutual orientation of the fields does not affect the structure of entanglement significantly.

Finally, the staggered field drastically changes the whole entanglement pattern. Qualitatively, the picture seems to be

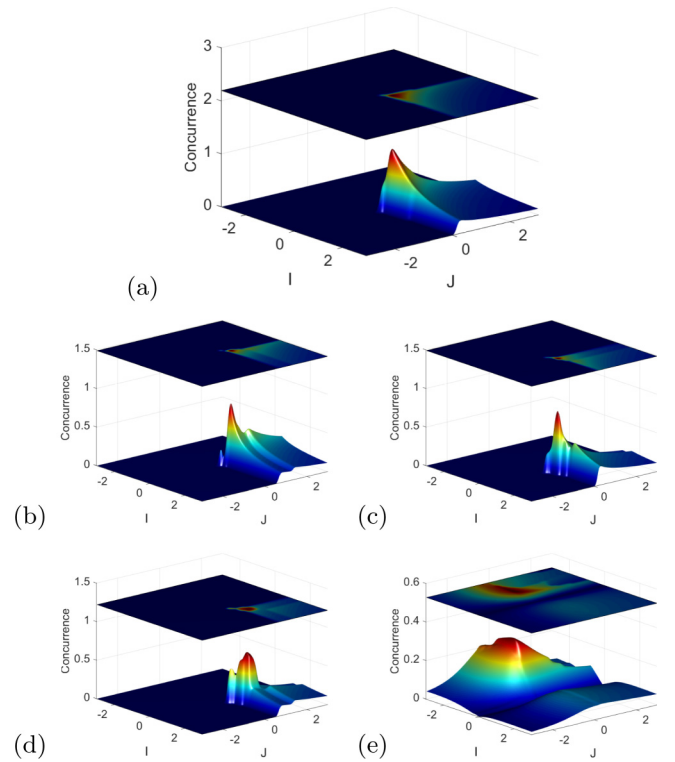


FIG. 6. Entanglement C (8) for intersubsystem exchange (4) $\sim (\hat{S}_i \hat{S}_j)(T_i^z T_j^z)$ with positive $K = +1$. At zero external fields, the entangled state is realized at the $J, J > 0$ domain. (a) $\mathcal{H}_s = \mathcal{H}_t \ll 1$. (b) $\mathcal{H}_s = 1, \mathcal{H}_t \ll 1$. (c) $\mathcal{H}_s \ll 1, \mathcal{H}_t = 1$. (d) $\mathcal{H}_s = 1$ and $\mathcal{H}_t = 1$. (e) Staggered fields $|\mathcal{H}_s| = |\mathcal{H}_t| = 1$ in both subsystems. Here, \mathcal{H}_s and \mathcal{H}_t stand for external fields in spin and pseudospin subsystems.

rotated from the zero-field case by $\pi/4$ counterclockwise. Significant entanglement appears in the half plane (pseudospin subsystem exchange $I < 0$).

At $K = +1$ [Figs. 6(a)–6(e)], the zero-field maximum entanglement is localized nearly at a single point, and when the external field is nonzero in one of the subsystems, there is a tendency to isolate the area of maximum entanglement from the rest of the region with zero entanglement. This tendency is especially pronounced for $\mathcal{H}_s \ll 1, \mathcal{H}_t = 1$ [see Fig. 6(c)]. When there are two nonzero external fields, a sharp peak in entanglement is formed near the origin [Fig. 6(c)] which is insensitive to the mutual orientation of the fields.

The effect of the staggered field (“counterclockwise rotation”), significant entanglement for $I < 0$), is similar to that for $K = -1$ except for inessential details. We cannot help mentioning that Figs. 5(e) and 6(e) resemble some of the works of Zaha Hadid.

B. Spin and pseudospin anisotropic interaction:

$$\hat{H}_{ts} = \sum (S_i^x S_j^x)(T_i^z T_j^z)$$

Here, we discuss the case when the intersubsystem interaction is even less symmetrical and has an Ising form in the parts in \hat{H}_{ts} referring to both spins and pseudospins. This is the Hamiltonian (1) and (2) with interaction between the subsystems (5). This interaction is the Ashkin-Teller one [41], although the model (1), (2), and (5) technically differs from

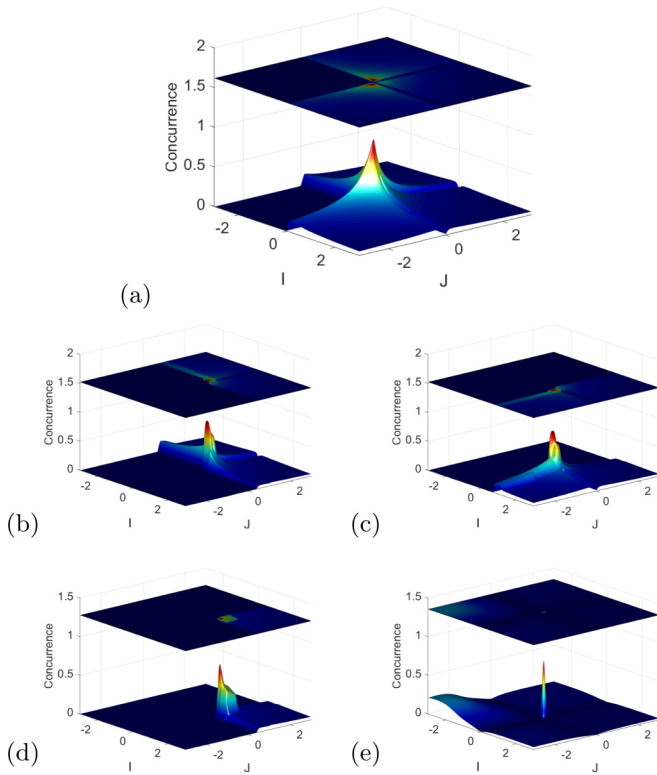


FIG. 7. Entanglement C (8) for intersubsystem exchange (5) $\sim (S_i^z S_j^z)(T_i^z T_j^z)$ with negative $K = -1$. At zero external fields, the entanglement is realized at 3/4 of the phase plane (except for the FM-FM region) with sharp maxima near the origin. When external field in the spin or pseudospin subsystem is nonzero, the entanglement in the corresponding quadrant disappears completely. (a) $\mathcal{H}_s = \mathcal{H}_t \ll 1$. (b) $\mathcal{H}_s = 1, \mathcal{H}_t \ll 1$. (c) $\mathcal{H}_s \ll 1, \mathcal{H}_t = 1$. (d) $\mathcal{H}_s = 1$ and $\mathcal{H}_t = 1$. (e) Staggered fields $|\mathcal{H}_s| = |\mathcal{H}_t| = 1$ in both subsystems. Here, \mathcal{H}_s and \mathcal{H}_t stand for external fields in spin and pseudospin subsystems.

the Ashkin-Teller model for which the exact solution exists [42].

The case of $K = -1$ is of special interest here. The entanglement is realized here at three quarters of the phase plane (two of the entanglement regions are, of course, symmetrical), and there are three sharp peaks near the origin; in addition, all areas of entanglement are separated by lines $J, I = 0$. For the opposite sign of the spin-pseudospin exchange $K = +1$, the entanglement pattern is realized, which is qualitatively similar to Fig. 6(a)—entanglement in the quarter of the phase diagram and the shark tooth near the origin (we will not give the corresponding figures).

Now, we address the nonzero field case. When the magnetic field is nonzero in one of the subsystems, the entanglement in the corresponding quadrant completely decays, and the situation in the other quadrants does not change qualitatively [with the increase of entanglement “edges” along one of the coordinate axes; see Figs. 7(b) and 7(c)]. When two external fields are nonzero simultaneously, a sharp peak is formed near the coordinate origin with weak entanglement in the quadrant $J > 0, I > 0$ and zero entanglement in the remaining regions [see Fig. 7(d)].

The effect of the staggered field is even more dramatic. The entanglement is almost or completely destroyed in the whole

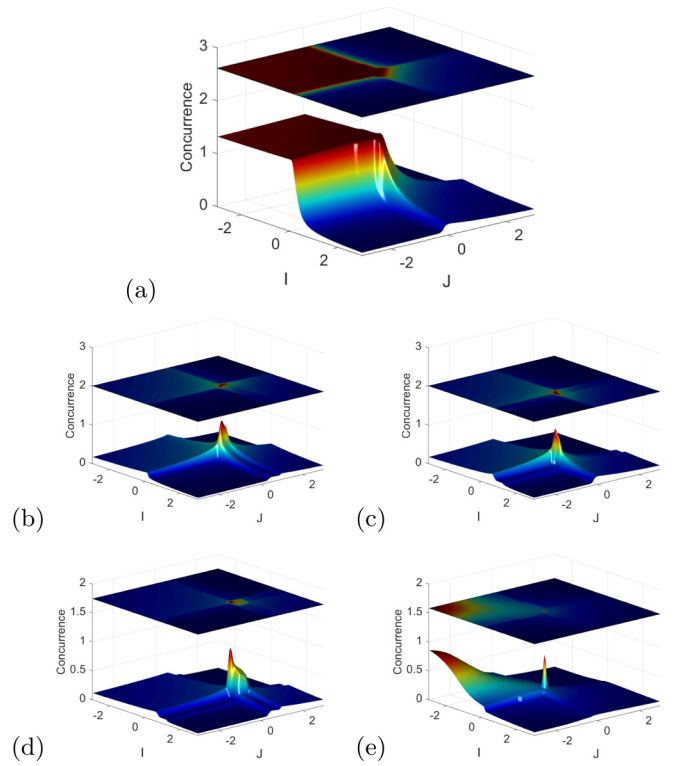


FIG. 8. Entanglement C (8) for intersubsystem exchange (6) $\sim (S_i^\alpha S_j^\alpha T_i^\alpha T_j^\alpha)$ with negative $K = -1$. At zero external fields, the superentanglement is formed in the FM-FM region of the phase plane. When external fields are nonzero, the entanglement disappears, leaving a sharp peak near the origin. (a) $\mathcal{H}_s = \mathcal{H}_t \ll 1$. (b) $\mathcal{H}_s = 1, \mathcal{H}_t \ll 1$. (c) $\mathcal{H}_s \ll 1, \mathcal{H}_t = 1$. (d) $\mathcal{H}_s = 1$ and $\mathcal{H}_t = 1$. (e) Staggered fields $|\mathcal{H}_s| = |\mathcal{H}_t| = 1$ in both subsystems. Here, \mathcal{H}_s and \mathcal{H}_t stand for external fields in spin and pseudospin subsystems.

phase plane, except the peak at the origin. Note, however, that the concurrence is nonzero in the $J < 0, I < 0$ quadrant.

The nonzero field case for the opposite sign, $K = +1$, differs in small details from the one just discussed, and we will not comment on it here.

C. Model interaction: $\hat{\mathbf{H}}_s = \sum (S_i^\alpha S_j^\alpha T_i^\alpha T_j^\alpha)$

Here, we consider an even more exotic case: a model interaction (6). This interaction looks very peculiar (and slightly resembles the compass model [43–45]); nevertheless, we discuss it for completeness of classification. With both signs of K , the most striking feature is the arising superentanglement at $J, I < 0$, that is, with both intersubsystem exchanges being ferromagnetic. The behavior of entanglement in the region $J, I > 0$ qualitatively (and semiquantitatively) resembles the case of Figs. 1(a) and 2(a).

Here, all the nonzero field cases are peculiar. When a magnetic field is nonzero in any of the subsystems, the entanglement in the corresponding quadrant dramatically decays, leaving mainly a sharp peak near the origin [see Figs. 8(b) and 8(c)]. The presence of magnetic fields in two subsystems results in a peak near the origin insensitive to the mutual direction of the fields [Fig. 8(d)].

The effect of the staggered field here looks like that in the model just considered [compare Figs. 8(e) and 7(e)]. The entanglement is almost or completely absent in the whole phase plane, except for the peak at the origin. The concurrence is considerable within the $J < 0, I < 0$ quadrant.

Since, as in the previous section, for $K = +1$, the concurrence structure appears to be qualitatively the same, we will not comment on that case.

VI. CONCLUSIONS

In this paper, the problem of quantum entanglement was addressed in terms of the behavior of finite chains described by different types of two-spin models. The analysis was performed by the exact diagonalization technique, allowing us to find comprehensive quantitative information concerning the systems under study. We were mainly focused on the behavior of concurrence, which is a good numerical measure of the entanglement. We determined the regions of pronounced entanglement at various relations between the characteristic parameters of the models. We have also revealed certain similarities in the behavior of concurrence and that of the two-site correlation functions (the latter can be considered a local indicator of entanglement).

We have also demonstrated the possibility to provide efficient control of the entanglement pattern by external fields (and by switching on nontrivial interactions). In particular, external fields can induce considerable entanglement in the areas where zero-field entanglement is clearly absent. On the other hand, the inverse effect is possible—the concerted action of the fields in both spin subsystems diminishing the entanglement.

We emphasize that due to the different physical origins of effective spin and pseudospin the applied fields may have a completely different nature, from the magnetic field to elastic stresses. For example, the simplest field-dependent part of a spin-orbital Hamiltonian has the form $hS^z + \Delta T^z$, where h is the magnetic field in energy units and Δ is the energy gap induced by local distortions [46]. Note that here the superscript

z correspond to the z axis in different spaces, spin and orbital ones. Depending on the ground state of the main Hamiltonian, such fields can affect the ground state in various ways, thus either enhancing or suppressing the entanglement.

The common experimental realization of the entanglement effects is related to the spin-orbital excitations, referred to as orbitons [47–52]. This issue has recently drawn additional interest in connection to the so-called Higgs and Goldstone modes in condensed-matter physics [53–55].

Ultracold atoms bring a new perspective to spin-orbital physics. Namely, a broad class of Hamiltonians of this type can be simulated not only in the framework of solid-state strongly correlated systems but also by ultracold atoms in the traps [22,23,56]. Then, the Kugel-Khomskii model can also involve an integer spin. In such experiments, a variety of artificial external fields can be introduced by tuning laser beams or by the trap geometry rearrangement.

However, the role of quantum entanglement in the spin-orbital (spin-pseudospin) excitations has not been addressed properly yet. We believe that our present work could be a good step forward in this direction.

ACKNOWLEDGMENTS

This work was supported by the Russian Foundation for Basic Research, Projects No. 19-02-00509 and No. 20-02-00015. K.I.K. acknowledges the support from the Russian Science Foundation, Project No. 20-62-46047. The work K.I.K. was partially performed during his stay at the Mikheev Institute of Metal Physics, Ural Branch, Russian Academy of Sciences, Ekaterinburg 620990, Russia. N.M.C. acknowledges the support from the Russian Science Foundation, Project No. 18-12-00438. The computations were carried out on MVS-10P at the Joint Supercomputer Center of the Russian Academy of Sciences (JSCC RAS). This work has been carried out also using computing resources of the federal collective usage center Complex for Simulation and Data Processing for Mega-Science Facilities at NRC “Kurchatov Institute”, [57].

-
- [1] G. Vidal, J. I. Latorre, E. Rico, and A. Kitaev, Entanglement in Quantum Critical Phenomena, *Phys. Rev. Lett.* **90**, 227902 (2003).
 - [2] R. Jozsa and N. Linden, On the role of entanglement in quantum-computational speed-up, *Proc. R. Soc. London, Ser. A* **459**, 2011 (2003).
 - [3] I. Bengtsson and K. Życzkowski, *Geometry of Quantum States: An Introduction to Quantum Entanglement* (Cambridge University Press, Cambridge, 2006).
 - [4] R. Horodecki, P. Horodecki, M. Horodecki, and K. Horodecki, Quantum entanglement, *Rev. Mod. Phys.* **81**, 865 (2009).
 - [5] M. E. Cuffaro and W. C. Myrvold, On the debate concerning the proper characterization of quantum dynamical evolution, *Philos. Sci.* **80**, 1125 (2013).
 - [6] M. Zidan, A.-H. Abdel-Aty, A. Younes, E. A. Zanaty, I. El-khayat, and M. Abdel-Aty, A novel algorithm based on entanglement measurement for improving speed of quantum algorithms, *Appl. Math. Inf. Sci.* **12**, 265 (2018).
 - [7] M.-C. Chen, R. Li, L. Gan, X. Zhu, G. Yang, C.-Y. Lu, and J.-W. Pan, Quantum-Teleportation-Inspired Algorithm for Sampling Large Random Quantum Circuits, *Phys. Rev. Lett.* **124**, 080502 (2020).
 - [8] E. P. G. Gale, Z. Mehdi, L. M. Oberg, A. K. Ratcliffe, S. A. Haine, and J. J. Hope, Optimized fast gates for quantum computing with trapped ions, *Phys. Rev. A* **101**, 052328 (2020).
 - [9] I. Georgescu, Trapped ion quantum computing turns 25, *Nat. Rev. Phys.* **2**, 278 (2020).
 - [10] A. L. Grimsmo, J. Combes, and B. Q. Baragiola, Quantum Computing with Rotation-Symmetric Bosonic Codes, *Phys. Rev. X* **10**, 011058 (2020).
 - [11] S. McArdle, S. Endo, A. Aspuru-Guzik, S. C. Benjamin, and X. Yuan, Quantum computational chemistry, *Rev. Mod. Phys.* **92**, 015003 (2020).
 - [12] A. Roggero, A. C. Li, J. Carlson, R. Gupta, and G. N. Perdue, Quantum computing for neutrino-nucleus scattering, *Phys. Rev. D* **101**, 074038 (2020).

- [13] B.-H. Wu, R. N. Alexander, S. Liu, and Z. Zhang, Quantum computing with multidimensional continuous-variable cluster states in a scalable photonic platform, *Phys. Rev. Research* **2**, 023138 (2020).
- [14] M. Josefsson and M. Leijnse, Double quantum-dot engine fueled by entanglement between electron spins, *Phys. Rev. B* **101**, 081408 (2020).
- [15] C. W. J. Beenakker, Electron-hole entanglement in the Fermi sea, in *Quantum Computers, Algorithms and Chaos, Proceedings of the International School of Physics “Enrico Fermi”* (IOS Press, Amsterdam, 2006), Vol. 162, pp. 307–347.
- [16] N. M. Chtchelkatchev, G. Blatter, G. B. Lesovik, and T. Martin, Bell inequalities and entanglement in solid-state devices, *Phys. Rev. B* **66**, 161320 (2002).
- [17] P. Hyllus, O. Gühne, D. Bruß, and M. Lewenstein, Relations between entanglement witnesses and Bell inequalities, *Phys. Rev. A* **72**, 012321 (2005).
- [18] K. I. Kugel and D. I. Khomskii, The Jahn-Teller effect and magnetism: Transition metal compounds, *Sov. Phys. Usp.* **25**, 231 (1982).
- [19] Y. Tokura and N. Nagaosa, Orbital physics in transition-metal oxides, *Science* **288**, 462 (2000).
- [20] A. Oleś, Fingerprints of spin-orbital entanglement in transition metal oxides, *J. Phys.: Condens. Matter* **24**, 313201 (2012).
- [21] W. Brzezicki, J. Dziarmaga, and A. Oleś, Exotic spin orders driven by orbital fluctuations in the Kugel-Khomskii model, *Phys. Rev. B* **87**, 064407 (2013).
- [22] A. M. Belemuk, N. M. Chtchelkatchev, A. V. Mikheyenkov, and K. I. Kugel, Magnetic phase diagram and quantum phase transitions in a two-species boson model, *Phys. Rev. B* **96**, 094435 (2017).
- [23] A. M. Belemuk, N. M. Chtchelkatchev, A. V. Mikheyenkov, and K. I. Kugel, Quantum phase transitions and the degree of nonidentity in the system with two different species of vector bosons, *New J. Phys.* **20**, 063039 (2018).
- [24] V. E. Valiulin, A. V. Mikheyenkov, K. I. Kugel, and A. F. Barabanov, Thermodynamics of symmetric spin-orbital model: One- and two-dimensional cases, *JETP Lett.* **109**, 546 (2019).
- [25] D. Gotfryd, E. M. Pärshcke, J. Chaloupka, A. M. Oleś, and K. Wohlfeld, How spin-orbital entanglement depends on the spin-orbit coupling in a Mott insulator, *Phys. Rev. Research* **2**, 013353 (2020).
- [26] E. Baldini, C. A. Belvin, M. Rodriguez-Vega, I. O. Ozel, D. Legut, A. Kozłowski, A. M. Oleś, K. Parlinski, P. Piekarczyk, J. Lorenzana *et al.*, Discovery of the soft electronic modes of the trimeron order in magnetite, *Nat. Phys.* **16**, 541 (2020).
- [27] R. Fumagalli, J. Heverhagen, D. Betto, R. Arpaia, M. Rossi, D. Di Castro, N. B. Brookes, M. Moretti Sala, M. Daghofer, L. Braicovich, *et al.*, Mobile orbitons in Ca_2CuO_3 : Crucial role of Hund’s exchange, *Phys. Rev. B* **101**, 205117 (2020).
- [28] Y. Chen, Z. D. Wang, Y. Q. Li, and F. C. Zhang, Spin-orbital entanglement and quantum phase transitions in a spin-orbital chain with $\text{SU}(2) \times \text{SU}(2)$ symmetry, *Phys. Rev. B* **75**, 195113 (2007).
- [29] W. Brzezicki, J. Dziarmaga, and A. Oleś, Topological Order in an Entangled $\text{SU}(2) \times \text{XY}$ Spin-Orbital Ring, *Phys. Rev. Lett.* **112**, 117204 (2014).
- [30] W.-L. You, P. Horsch, and A. Oleś, Quantum entanglement in the one-dimensional spin-orbital $\text{SU}(2) \times \text{XXZ}$ model, *Phys. Rev. B* **92**, 054423 (2015).
- [31] W.-L. You, A. Oleś, and P. Horsch, von Neumann entropy spectra and entangled excitations in spin-orbital models, *Phys. Rev. B* **86**, 094412 (2012).
- [32] A. Lüscher and A. M. Läuchli, Exact diagonalization study of the antiferromagnetic spin-1/2 Heisenberg model on the square lattice in a magnetic field, *Phys. Rev. B* **79**, 195102 (2009).
- [33] D. Medvedeva, S. Isakov, F. Krien, V. V. Mazurenko, and A. I. Lichtenstein, Exact diagonalization solver for extended dynamical mean-field theory, *Phys. Rev. B* **96**, 235149 (2017).
- [34] S. Schiffer, J. Wang, X.-J. Liu, and H. Hu, Many-body localization in XY spin chains with long-range interactions: An exact-diagonalization study, *Phys. Rev. A* **100**, 063619 (2019).
- [35] Y. Wang, J. P. Dehollain, F. Liu, U. Mukhopadhyay, M. S. Rudner, L. M. K. Vandersypen, and E. Demler, *Ab initio* exact diagonalization simulation of the Nagaoka transition in quantum dots, *Phys. Rev. B* **100**, 155133 (2019).
- [36] A. Tanaka, Metal-insulator transition in the two-dimensional Hubbard model: Dual fermion approach with Lanczos exact diagonalization, *Phys. Rev. B* **99**, 205133 (2019).
- [37] J. R. Johansson, P. D. Nation, and F. Nori, QuTiP: An open-source Python framework for the dynamics of open quantum systems, *Comput. Phys. Commun.* **183**, 1760 (2012).
- [38] J. R. Johansson, P. D. Nation, and F. Nori, QuTiP 2: A Python framework for the dynamics of open quantum systems, *Comput. Phys. Commun.* **184**, 1234 (2013).
- [39] J. van den Brink, W. Stekelenburg, D. I. Khomskii, G. A. Sawatzky, and K. I. Kugel, Elementary excitations in the coupled spin-orbital model, *Phys. Rev. B* **58**, 10276 (1998).
- [40] See Supplemental Material at <http://link.aps.org/supplemental/10.1103/PhysRevB.102.155125> for quantum entanglement, local indicators, and the effect of external fields in the Kugel-Khomskii model.
- [41] J. Ashkin and E. Teller, Statistics of Two-Dimensional Lattices with Four Components, *Phys. Rev.* **64**, 178 (1943).
- [42] K. I. Kugel and D. I. Khomskii, Orbital degeneracy and some one-dimensional two-spin models, *Sov. J. Low Temp. Phys.* **6**, 99 (1980).
- [43] W. Brzezicki, J. Dziarmaga, and A. M. Oleś, Quantum phase transition in the one-dimensional compass model, *Phys. Rev. B* **75**, 134415 (2007).
- [44] E. Eriksson and H. Johannesson, Multicriticality and entanglement in the one-dimensional quantum compass model, *Phys. Rev. B* **79**, 224424 (2009).
- [45] G. Jackeli and G. Khaliullin, Mott Insulators in the Strong Spin-Orbit Coupling Limit: From Heisenberg to a Quantum Compass and Kitaev Models, *Phys. Rev. Lett.* **102**, 017205 (2009).
- [46] S. V. Streltsov and D. I. Khomskii, Orbital physics in transition metal compounds: New trends, *Phys. Usp.* **60**, 1121 (2017).
- [47] E. Saitoh, S. Okamoto, K. T. Takahashi, K. Tobe, K. Yamamoto, T. Kimura, S. Ishihara, S. Maekawa, and Y. Tokura, Observation of orbital waves as elementary excitations in a solid, *Nature (London)* **410**, 180 (2001).
- [48] J. van den Brink, Orbital Excitations in LaMnO_3 , *Phys. Rev. Lett.* **87**, 217202 (2001).
- [49] S. Ishihara, Y. Murakami, T. Inami, K. Ishii, J. Mizuki, K. Hirota, S. Maekawa, and Y. Endoh, Theory and experiment of orbital excitations in correlated oxides, *New J. Phys.* **7**, 119 (2005).
- [50] Y. Tanaka, A. Q. R. Baron, Y.-J. Kim, K. J. Thomas, J. P. Hill, Z. Honda, F. Iga, S. Tsutsui, D. Ishikawa, and C. S. Nelson,

- Search for orbitons in LaMnO_3 , YTiO_3 and KCuF_3 using high-resolution inelastic x-ray scattering, *New J. Phys.* **6**, 161 (2004).
- [51] K. P. Schmidt, M. Gruninger, and G. S. Uhrig, Fate of orbitons coupled to phonons, *Phys. Rev. B* **76**, 075108 (2007).
- [52] E. Benckiser, R. Ruckamp, T. Moller, T. Taetz, A. Moller, A. A. Nugroho, T. T. M. Palstra, G. S. Uhrig, and M. Gruninger, Collective orbital excitations in orbitally ordered YVO_3 and YVO_3 , *New J. Phys.* **10**, 053027 (2008).
- [53] N. N. Kovaleva, O. E. Kusmartseva, K. I. Kugel, A. A. Maksimov, D. Nuzhnyy, A. M. Balbashov, E. I. Demikhov, A. Dejneka, V. A. Trepakov, F. V. Kusmartsev, *et al.*, Anomalous multi-order Raman scattering in LaMnO_3 : A signature of quantum lattice effects in a Jahn–Teller crystal, *J. Phys.: Condens. Matter* **25**, 155602 (2013).
- [54] D. M. Juraschek, Q. N. Meier, and P. Narang, Parametric Excitation of an Optically Silent Goldstone-Like Phonon Mode, *Phys. Rev. Lett.* **124**, 117401 (2020).
- [55] Q. N. Meier, A. Stucky, J. Teyssier, S. M. Griffin, D. van der Marel, and N. A. Spaldin, Manifestation of structural Higgs and Goldstone modes in the hexagonal manganites, *Phys. Rev. B* **102**, 014102 (2020).
- [56] C. Gross and I. Bloch, Quantum simulations with ultracold atoms in optical lattices, *Science* **357**, 995 (2017).
- [57] <http://ckp.nrcki.ru/>.